

Marquette University  
**e-Publications@Marquette**

---

Chemistry Faculty Research and Publications

Chemistry, Department of

---

5-1-2009

# Variation of anions in layered double hydroxides: Effects on dispersion and fire properties

Linjiang Wang  
*Marquette University*

Shengpei Shu  
*Hunan Normal University*

Dan Chen  
*Hunan Normal University*

Charles A. Wilkie  
*Marquette University, [charles.wilkie@marquette.edu](mailto:charles.wilkie@marquette.edu)*

---

Accepted version. *Polymer Degradation and Stability*, Vol. No. 5 (May 2009): 770-781. DOI. © 2009 Elsevier Ltd. Used with permission.

Marquette University

e-Publications@Marquette

***Chemistry Faculty Research and Publications/College of Arts and Sciences***

***This paper is NOT THE PUBLISHED VERSION; but the author's final, peer-reviewed manuscript.*** The published version may be accessed by following the link in the citation below.

*Polymer Degradation and Stability*, Vol. 94, No. 4 (April 2009): 496-505. [DOI](#). This article is © Elsevier and permission has been granted for this version to appear in [e-Publications@Marquette](#). Elsevier does not grant permission for this article to be further copied/distributed or hosted elsewhere without the express permission from Elsevier.

# Variation of Anions in Layered Double Hydroxides: Effects on Dispersion and Fire Properties

Linjiang Wang

Department of Chemistry and Fire Retardant Research Facility, Marquette University, Milwaukee, WI

Shengpei Su

Department of Chemistry and Chemical Engineering, Hunan Normal University, Changsha 410081, China

Dan Chen

Department of Chemistry and Chemical Engineering, Hunan Normal University, Changsha 410081, China

Charles A. Wilkie

Department of Chemistry and Fire Retardant Research Facility, Marquette University, Milwaukee, WI

## Abstract

Layered double hydroxides (LDHs) are interesting materials for nanocomposite formation because one can vary the identity of the metals, the anions and the stoichiometry to see the effect of these on the ability of the nanomaterial to disperse in a polymer and to see what effect dispersion has on the properties of the polymer. In this study, the anions 2-ethylhexyl sulfate (SEHS), bis(2-ethylhexyl) phosphate (HDEHP) and dodecyl benzenesulfonate (SDBS) have been utilized as the charge balancing anions to synthesize organo-LDHs. Nanocomposites of poly(methyl methacrylate) (PMMA) and polystyrene (PS) with organo-LDHs were prepared both by melt blending and bulk polymerization. X-ray diffraction and transmission electron microscopy were used to characterize the morphology of the nanocomposites while the thermal stability and fire properties of

nanocomposites were studied by thermogravimetric analysis and cone calorimetry; the mechanical properties are also investigated. In general, it is easier to disperse these organo-LDHs in PMMA than in PS, but the sulfate cannot be dispersed at the nanometer level in either material. The addition of these organo-LDHs does not affect the mechanical properties. The best fire properties are obtained with the sulfonate LDH, SDBS; the reduction in the peak heat release rate is almost 50% for both polymers.

## Keywords

Anions, Dispersion, Flame retardance, Poly(methyl methacrylate), Polystyrene, LDH nanocomposite

## 1. Introduction

In recent years, the development of halogen-free flame retardants for polymeric materials with low emission of smoke and hazardous gases has become more and more important. Magnesium hydroxide (MDH) and alumina trihydrate (ATH) are well-known fire retardants, which are attractive because of their low price and good performance; the limitation of MDH and ATH is that high loadings are required to achieve good fire retardant performance and these high loadings will cause significant degradation in mechanical properties.

Layered double hydroxides (LDHs), also called hydrotalcites or anionic clays, are new and promising layered materials for preparing multifunctional polymer/inorganic nanocomposites [\[1\]](#), [\[2\]](#). One of the interesting properties for layered double hydroxides is that the identity of both the divalent and the trivalent metal ions and their ratio, as well as the identity of the anion, are adjustable to obtain different charge densities and interlayer spacing. The general formula of an LDH is  $[M^{2+}_{1-x}M^{3+}_x(OH)_2]A^{n-}_{x/n}mH_2O$ , where M is  $Li^+$  or a divalent cation such as  $Ca^{2+}$ ,  $Mg^{2+}$ ,  $Ni^{2+}$ ,  $Co^{2+}$ ,  $Zn^{2+}$ ,  $Mn^{2+}$  or  $Cu^{2+}$ ,  $M^{3+}$  is a trivalent cation such as  $Al^{3+}$ ,  $Cr^{3+}$ ,  $Co^{3+}$ ,  $Ni^{3+}$ ,  $Mn^{3+}$ ,  $Fe^{3+}$ ,  $V^{3+}$  or  $Ga^{3+}$ , and A is an interlayer anion such as  $Cl^-$ ,  $NO_3^-$ ,  $ClO_4^-$ ,  $CO_3^{2-}$ ,  $SO_4^{2-}$  or organic anions [\[3\]](#). LDHs have positive charge on the brucite-like sheets compensated by interlayer anions. An LDH possesses a similar structure and composition as MDH and ATH, which makes them promising for applications as thermal stabilizers and flame retardants. An LDH is preferred over MDH and ATH because it can generate water both by loss of interlayer water and by decomposition of the OH groups in the brucite-like layer [\[4\]](#). Although there are not large deposits of LDHs, compared to the cationic clays [\[5\]](#), they have received considerable attention in recent years because of their special structure and properties, ease of synthesis in the laboratory and their potential industrial uses, including as fire retardants [\[6\]](#), [\[7\]](#), [\[8\]](#).

The field of polymer/inorganic nanocomposites has attracted considerable attention for their novel or enhanced properties due to nanometer dispersion of the inorganic compound in the polymer matrix. The homogeneous distribution of stacks of clay layers, at the nanometer level in a polymer, gives a nanocomposite which can be either intercalated, if the registry between the clay layers is maintained, or exfoliated, if this registry is lost [\[9\]](#). A third possibility is an immiscible nanocomposite, also known as a microcomposite or conventional composite, in which the clay is merely a filler and is not well-dispersed. It is difficult to obtain dispersion at the nanometer level with an LDH because of the high charge density, small gallery height and strong hydrophilicity. Monomer and polymer molecules cannot easily penetrate the LDH layers nor can LDH layers be easily homogeneously dispersed in a hydrophobic polymer matrix. Accordingly, the pristine LDHs have to be modified with organic anions and many kinds of anions have been successfully intercalated into LDHs to study the influence on properties of nanocomposites, including the common inorganic anions, carboxylates, sulfates, polymeric anions, and complex anions, such as polyoxometalate [\[10\]](#), [\[11\]](#). The influence of the metal ions and linear alkyl carboxylates in organo-LDH on fire properties of PMMA and PS has been reported in previous work from this laboratory [\[12\]](#), [\[13\]](#), [\[14\]](#). There are few reports comparing different kinds of organic anions on the dispersion of organo-LDHs in polymers and the fire properties of polymer nanocomposites.

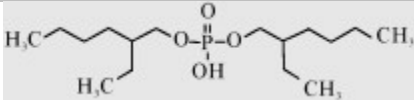
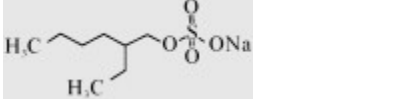
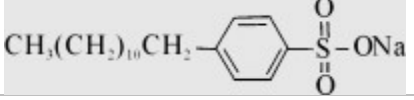
The objective of this research is to examine the effect of various types of organic anions on the properties of LDHs, including its dispersability, thermal and fire properties and mechanical properties with poly(methyl methacrylate) and polystyrene. The anions used are 2-ethylhexyl sulfate (SEHS), bis(2-ethylhexyl) phosphate (HDEHP) and dodecyl benzenesulfonate (SDBS).

## 2. Experimental

### 2.1. Materials

$\text{Al}(\text{NO}_3)_3 \cdot 9\text{H}_2\text{O}$  (reagent grade),  $\text{Mg}(\text{NO}_3)_2 \cdot 6\text{H}_2\text{O}$  (reagent grade), NaOH (reagent grade), sodium 2-ethylhexyl sulfate (50% in water), poly(methyl methacrylate) (reagent grade), with typical  $M_w$  120,000, polystyrene (reagent grade), with  $M_w$  192,000, monomeric styrene and methyl methacrylate, initiator benzoyl peroxide (BPO) (97%) were purchased from the Aldrich Chemical Company. Sodium bis(2-ethylhexyl) phosphate (reagent grade 97%), and sodium dodecyl benzenesulfonate (reagent grade 98%), were obtained from TCI America. All of the materials were used as received without further purification. The structures of the organic anions are shown in [Table 1](#).

Table 1. The structures of different anions used for interaction within the LDH.

Chemical name	Structure	Symbol of the anions
Bis(2-ethylhexyl) phosphate		HDEHP
Sodium 2-ethylhexyl sulfate		SEHS
Sodium dodecyl benzenesulfonate		SDBS

### 2.2. Preparation of organo-LDHs

The organo-LDHs were prepared by the co-precipitation following, with minor adaptations, the method of Zhao and Kathryn [3]. In a 3-L three-neck round bottom flask equipped with a stirrer, addition funnel, pH probe and a condenser were placed 51.3 g (0.200 mol) of  $\text{Mg}(\text{NO}_3)_2 \cdot 6\text{H}_2\text{O}$  and 37.5 g (0.100 mol) of  $\text{Al}(\text{NO}_3)_3 \cdot 9\text{H}_2\text{O}$  in 240 mL of degassed water. The reaction must be kept free from carbon dioxide so as to prevent the formation of a carbonate so all manipulations were carried out using well-degassed water and the reaction was conducted under a nitrogen atmosphere to exclude  $\text{CO}_2$ . To the above solution was added drop-wise 1200 mL of solution containing 0.15 mol of SEHS (62 mL), or SDBS (65 g), or NaDEHP (52 mL, formed by reaction of the free acid with NaOH), while maintaining the pH around 10.0 with vigorous stirring at 65 °C. The resulting white precipitate was aged in the mother liquid for 48 h at 65 °C, and then filtered to remove all of the supernatant liquid. Decarbonated and deionized water was used and  $\text{N}_2$  was bubbled throughout the process to minimize  $\text{CO}_2$ . The sample was washed several times with large amounts of deionized/degassed water and was dried at 50 °C in a vacuum oven for 24 h.

Magnesium aluminum nitrate layered double hydroxide ( $\text{MgAl-NO}_3\text{-LDH}$ ) was also synthesized by the co-precipitation method. A solution of 51.3 g (0.200 mol) of  $\text{Mg}(\text{NO}_3)_2 \cdot 6\text{H}_2\text{O}$  and 37.5 g (0.100 mol) of  $\text{Al}(\text{NO}_3)_3 \cdot 9\text{H}_2\text{O}$  in 240 mL of decarbonated and deionized water was added drop-wise to a solution of 24 g (0.60 mol) of NaOH and 34 g (0.40 mol) of  $\text{NaNO}_3$  in 300 mL of decarbonated/deionized water under vigorous stirring at pH 10.0. The sample was aged for 24 h at 65 °C, followed by washing several times using decarbonated/deionized water and then drying at 50 °C in a vacuum oven for 24 h.

### 2.3. Preparation of nanocomposites

The nanocomposites were prepared both by melt blending and bulk polymerization. For melt blending, the polymer (PMMA or PS) and the organo-LDHs were pre-mixed in a beaker (the content of the organo-LDHs in mixture was 3%, 5% and 10%), then melt blended in Brabender Plasticorder at 185 °C for 10 min at 60 rpm. The mixture was removed from the mixer and cut into pieces for use. For bulk polymerization, in a 400 mL beaker were placed 3 g, 5 g or 10 g of HDEHP-LDH, 0.5 g of benzoyl peroxide as radical initiator, and 100 g of styrene or methyl methacrylate monomer. The mixture was stirred at room temperature under flowing  $\text{N}_2$  gas for 12 h until it became homogeneous. The homogeneous system was heated at 80 °C to obtain a prepolymer, then

polymerized at 70 °C for 48 h. The product was dried under vacuum for 12 h at 100 °C to obtain the nanocomposite. The molecular weight of the PS and PMMA were ca. 188,300 and 123,700, respectively, obtained from viscosity data.

## 2.4. Characterization

X-ray diffraction was performed on a Rigaku Miniflex II desktop X-ray powder diffractometer with Cu K $\alpha$  generator ( $\lambda = 0.15404$  nm), accelerating voltage was 50 kV at a current of 20 mA. Scans were taken at  $2\theta = 2-70^\circ$  at 0.1 step size. Polymer composite samples were pressed into  $20 \times 15 \times 1$  mm<sup>3</sup> thickness plaques by compression molding. FTIR spectroscopic analyses were carried out on a Nicolet 560 Fourier transform infrared spectrometer using the KBr method. Spectra were recorded between 400 and 4000 cm<sup>-1</sup> at a resolution of 4 cm<sup>-1</sup>. Thermogravimetric analysis (TGA) was performed on an SDT 2960 machine at 12–14 mg scale under a flowing nitrogen atmosphere at a ramp rate of 20 °C/min. All TGA samples were run in duplicate and the average values are reported; the reproducibility of temperature is  $\pm 2$  °C and mass is reproducible to  $\pm 0.4\%$ . Cone calorimetry was performed on an Atlas CONE-2 according to ASTM E 1354 at an incident flux of 50 kW/m<sup>2</sup> for PMMA system and 35 kW/m<sup>2</sup> for PS system using a cone shaped heater, exhaust flow was set at 24 L/s; all samples were burned in triplicate. Cone samples (about 30 g) were prepared by compression molding into  $100 \times 100 \times 3$  mm<sup>3</sup> square plaques. Based on many thousands of samples that have been run, cone measurements are considered to have error bars of  $\pm 10\%$ . The TEM imaging was carried out using a transmission electron microscope JEOL 1230 with an accelerating voltage of 100 kV. The samples were ultramicrotomed with a glass knife on an AO-E microtome at room temperature to give sections of  $\sim 90$  nm in thickness. The sections were transferred from the knife-edge to Cu grids. The tensile mechanical properties were obtained on an Instron 5500 series test instrument at room temperature. Rectangular strip specimens with a thickness of 1.7 mm, prepared with a CS-183MMX Min Max Molder injection machine, were used for tensile testing. The crosshead speed of the tester was 5 mm/min. The strain was calculated from the displacement of the crosshead. A minimum of six specimens were tested for each data point and the averages are reported.

## 3. Results and discussion

### 3.1. Organo-LDHs

#### 3.1.1. X-ray diffraction (XRD) studies

[Fig. 1](#) shows the XRD patterns of pristine MgAl–NO<sub>3</sub>–LDH ([Fig. 1A](#)) along with that of SDBS-LDH ([Fig. 1B](#)), SEHS-LDH ([Fig. 1C](#)) and HDEHP-LDH ([Fig. 1D](#)). The basal spacings are 0.77 nm, 2.90 nm, 2.14 nm and 2.34 nm, respectively; all of these show several orders of diffraction, indicating a well-layered structure. The change in  $d$ -spacing indicates the successful intercalation of SDBS, SEHS and HDEHP and the well-ordered arrangement of organic molecules in the interlayer of LDHs. The value for SDBS-LDH corresponds well to those reported in the literature for these materials [\[15\]](#), [\[16\]](#), but the value of HDEHP-LDH is larger than that in the literature, which was 1.52 nm [\[16\]](#).

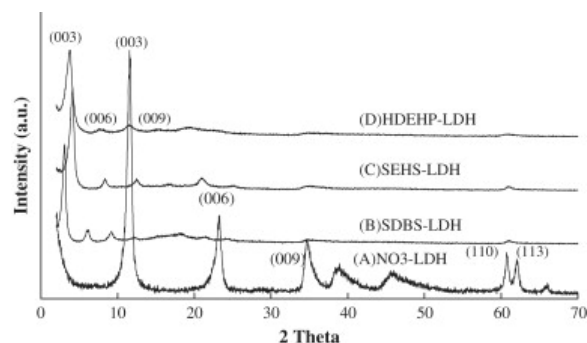


Fig. 1. XRD patterns of layered double hydroxides (LDHs) with (A) intercalated NO<sub>3</sub><sup>-</sup>, (B) SDBS, (C) SEHS and (D) HDEHP.

The lengths of the backbones of SDBS, SEHS and HDEHP are 2.1 nm, 0.98 nm and 0.95 nm (with double tail structure), respectively, calculated using Spartan with an STO-3G basis set, and the gallery heights of the corresponding organo-LDHs are 2.41 nm, 1.66 nm and 1.86 nm. Gallery height is the basal spacing minus the size of the LDH platelet (4.77 Å) [17]. The interlayer gallery height of SDBS-LDH is close to the size of anion SDBS considering the Van der Waals radii of the end atoms; for SEHS-LDH, the interlayer gallery height is much larger than the size of SEHS; HDEHP contains one negatively charged end  $\text{PO}_4^-$  and two branched hydrocarbon chains with a length of 0.95 nm for one branch. It is suggested that the negative end of the anion contacts the positively charged layer of the LDH with the tails pointing to the center of the interlayer. It is reasonable that SEHS and HDEHP chains form a bilayer with  $56^\circ$  and  $70^\circ$  tilt angles, respectively, in which there is no SEHS and HDEHP overlap (Fig. 2A and B), SDBS has similar vertical monolayer arrangement with the long chain axis perpendicular to the interlamellar surface (Fig. 2C).

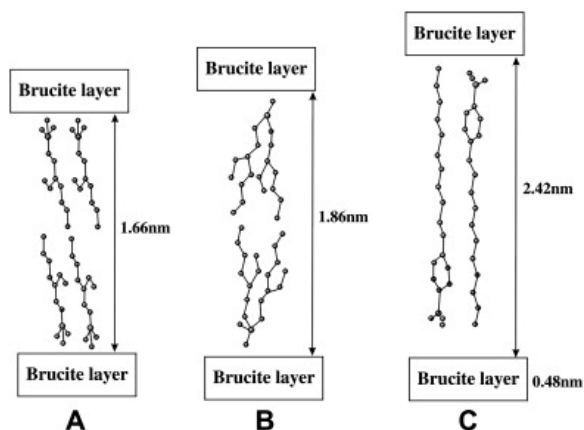


Fig. 2. Arrangement of SEHS (A), HDEHP (B) and SDBS (C) in the interlayer of LDHs.

### 3.1.2. Fourier transform infrared (FTIR) spectral studies

The Fourier transform infrared spectra of the organo-LDHs consist of two types of vibrations, one corresponding to the intercalated anions and the other to the pristine LDH (Fig. 3). All samples show a broad intense band centered at  $3500\text{ cm}^{-1}$  due to the OH stretching mode of layer hydroxyl groups and of interlayer water molecules. The bending mode of water molecules is responsible for the weak band at  $1640\text{ cm}^{-1}$ . A strong peak at  $1380\text{ cm}^{-1}$  for  $\text{MgAl-NO}_3\text{-LDH}$  (Fig. 3A) is associated with the stretching vibration of  $\text{N}=\text{O}$  in the nitrate anion [18]. A weak adsorption in the spectrum of organo-LDHs at  $1384\text{ cm}^{-1}$  may suggest the presence of a small amount of nitrate or the band may also be attributed to  $\text{CH}_3$  symmetrical bend vibration [19]. All the organo-LDHs exhibited strong absorption bands in the range of  $2950\text{--}2960\text{ cm}^{-1}$  and  $2870\text{--}2880\text{ cm}^{-1}$  which are attributed to the asymmetric  $\text{CH}_3$  and  $\text{CH}_2$  stretching vibration, respectively. The band  $1470\text{ cm}^{-1}$  is attributed to CH bending vibration [6]. The functional groups of the surfactants also exhibit their characteristic FTIR bands. In HDEHP-LDH, the characteristic  $\text{P-O-C}$  stretching vibration band at  $1100\text{ cm}^{-1}$ , and the  $\text{P}=\text{O}$  stretching vibration are indicated by a band at  $1250\text{ cm}^{-1}$  (Fig. 3B). For SDBS-LDH, the symmetric and asymmetric stretching vibration of  $\text{S}=\text{O}$  appeared at  $1040\text{ cm}^{-1}$  and  $1190\text{ cm}^{-1}$ , respectively (Fig. 3C), while the corresponding bands in SEHS-LDH appeared at  $1070\text{ cm}^{-1}$  and  $1225\text{ cm}^{-1}$ , respectively (Fig. 3D).

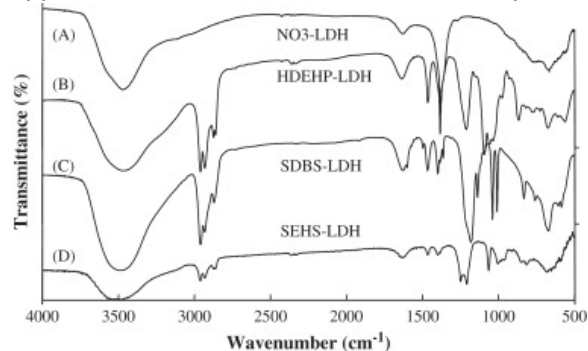


Fig. 3. FTIR spectra for (A) layered double hydroxides with intercalated NO<sub>3</sub>, (B) HDEHP, (C) SDBS and (D) SEHS.

### 3.1.3. Thermogravimetric analysis (TGA) studies

Fig. 4 illustrates the TGA curves of MgAl–NO<sub>3</sub>-LDH, SEHS-LDH, HDEHP-LDH and SDBS-LDH. For the MgAl–NO<sub>3</sub>-LDH (Fig. 4D), the first weight loss stage, up to 190 °C, is due to the loss of physisorbed and interlayer water molecules; the weight loss is about 13%. The second stage, up to 400 °C, is due to the conversion of hydroxyl groups of the brucite-like layers into oxide groups; the weight loss is about 32% [20].

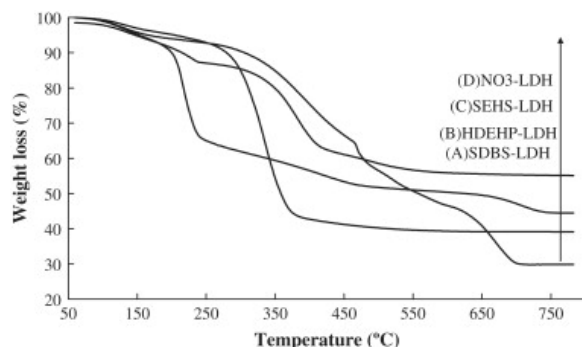


Fig. 4. TGA profiles for (A) layered double hydroxides with intercalated NO<sub>3</sub>, (B) SEHS, (C) HDEHP and (D) SDBS.

For the organo-LDHs, the first weight loss stage, up to 190 °C, is similar to that of the pristine LDH. The second stage is different because of the different stability and organic content in the interlayer. In this region, the organic anions and the LDH degradation will occur.

## 3.2. Dispersion of organo-LDHs in PMMA and PS

### 3.2.1. XRD characterization

Generally, the formation of an intercalated nanocomposite results in an increase in basal spacing in the XRD pattern, while the formation of an exfoliated nanocomposite leads to the complete loss of registry between the layers and therefore no peak can be observed. The presence of an XRD peak at a lower  $2\theta$  implies the formation of an intercalated structure, while the absence of a peak may be indicative of either exfoliation or a disordered immiscible structure [21]. The presence of a small, diffuse peak may suggest a mixed intercalated-disordered structure [22]. Fig. 5 shows the XRD patterns of the polymer/organo-LDH composites by melt blending. The basal spacing of HDEHP-LDH is 2.34 nm. After melt blending with PMMA at 3%, 5%, and 10% organo-LDH loading, no peak is observed in the composite (Fig. 5a), which suggests that HDEHP-LDH may have good dispersion and an exfoliated structure or disordering and an immiscible structure. When HDEHP-LDH is melt blended with PS, a broad and weak peak near the basal spacing of 2.44 nm is evident (Fig. 5d) which is only a small increase from that in the pristine LDH and is likely indicative of disordering and poor dispersion.

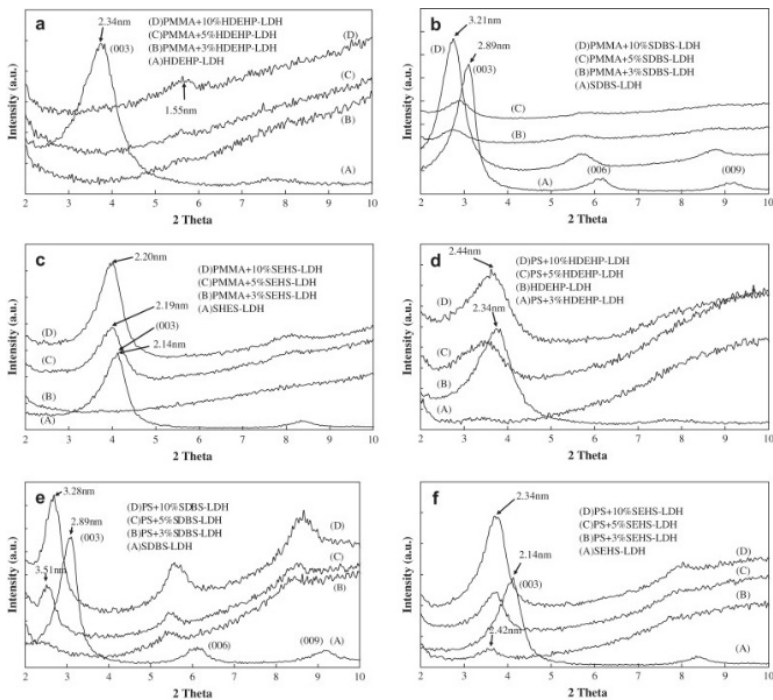


Fig. 5. XRD patterns of PMMA with (a) HDEHP-LDH, (b) SDBS-LDH, (c) SEHS-LDH; PS with (d) SDBS-LDH, (e) HDEHP-LDH, (f) SEHS-LDH by melt blending.

The basal spacing for SDBS-LDH has increased in the PMMA composite from 2.89 nm to 3.21 nm (Fig. 5B) and in PS composite from 2.89 nm to 3.28 nm (Fig. 5e). The increase in basal spacing may be due to the intercalation of polymer into the interlayer region of LDH, induced by the shear during melt blending. At 10% SDBS-LDH loading, a strong peak is evident, but at 3% and 5% loading, the (003) peaks are weak and broad, which suggest a mixed disordered/intercalated structure for SDBS-LDH in PMMA and PS.

The XRD patterns of PMMA/SEHS-LDH composite and PS/SEHS-LDH composite show peaks at similar position as the pristine SEHS-LDH, corresponding to a basal spacing of 2.14–2.34 nm (Fig. 5c and f); the small increase in the *d*-spacing suggests poor dispersion of SEHS-LDH in PMMA and PS.

Fig. 6 shows the XRD patterns of polymer/HDEHP-LDH composites by bulk polymerization. There is essentially no increase in the basal spacing of HDEHP-LDH in PMMA and PS composites. The (003) peak of HDEHP-LDH in PMMA almost disappeared, but the weak broad peak shows a decrease of basal spacing (Fig. 6a). The basal spacing of HDEHP-LDH in PS is very similar to the original HDEHP-LDH (Fig. 6b). In general, bulk polymerization is not as successful with an LDH as with MMT, perhaps because the LDH does not disperse as well in an organic solvent (or the monomer) as does MMT. When these, or other, LDHs have been placed in organic solvents and stirred for a time period, it is found that the LDH will settle out of the solvent rather quickly after the stirring is stopped. On the other hand, with an MMT the clay stays suspended for quite a long time.

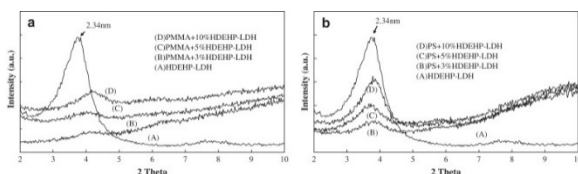


Fig. 6. XRD patterns of PMMA with (a) HDEHP-LDH and (b) PS with HDEHP by bulk polymerization.

### 3.2.2. Morphology by TEM

The XRD results give useful information on the state of organo-LDHs in the polymer but do not provide a complete picture of the morphology. TEM is required to complement this information to enable the evaluation of the dispersion of LDH in the polymers. In general, both a lower magnification image, to show the global



dispersion of the LDH in the polymers, and a higher magnification image, to evaluate the registry of the layer are needed. The morphologies of the PMMA (nano)composites with 5% organo-LDH loading are shown in [Fig. 7](#); the lower magnification image is shown on the left and higher on the right. One can observe a fair degree of delamination in PMMA/HDEHP-LDH composite ([Fig. 7a](#) and b) and PMMA/SDBS-LDH composite ([Fig. 7c](#) and d) and it is reasonable to describe these materials as exfoliated; single LDH layers, evidence for exfoliation, are present in abundance throughout the polymer matrix. There is no significant orientation of these platelets. In contrast, when SEHS-LDH is melt blended with PMMA, intercalated layers co-exist with large agglomerated LDH; SEHS-LDH has poorer dispersion in PMMA than HDEHP-LDH and SDBS-LDH ([Fig. 7e](#) and f).

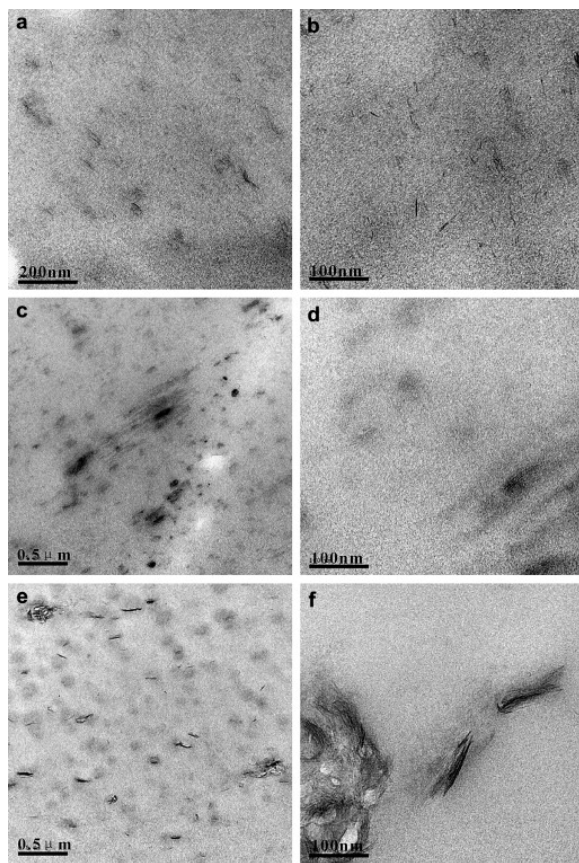


Fig. 7. TEM micrographs of melt blended PMMA with: (a, b) phosphate LDH, HDEHP; (c, d) sulfonate LDH, SDBS and (e, f) the sulfate LDH, SEHS. The low magnification image is shown on the left with the higher magnification image on the right.

For PS, the agglomerated tactoids of LDH are observed in the lower magnification PS/HDEHP-LDH ([Fig. 8g](#)) and PS/SEHS-LDH composites ([Fig. 8k](#)); PS-sulfate shows larger agglomerates than PS-phosphate. The higher magnification TEM image of PS-phosphate and PS-sulfate shows some evidence of intercalation ([Fig. 8h](#) and l); nonetheless, based on the low magnification images, these must be described as immiscible or microcomposites. SDBS-LDH, the sulfonate, with a mixed exfoliated-intercalated structure ([Fig. 7i, j](#)), shows better dispersion in PS than either the phosphate or the sulfate.

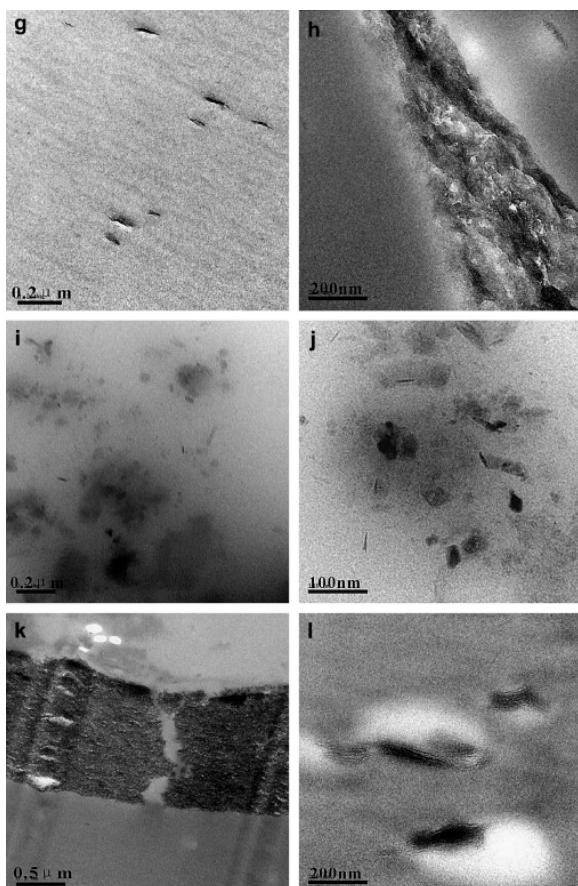


Fig. 8. TEM micrographs of melt blended PS composites with: (g, h) phosphate LDH, HDEHP, (i, j) sulfonate LDH, SDBS and (k, l) sulfate LDH, SEHS. The low magnification image is shown on the left with the higher magnification image on the right.

The morphological features observed in [Fig. 7](#), [Fig. 8](#) give a clear understanding of the mechanism of exfoliation of the organo-LDH during melt blending. At first, the polymer chain or segments penetrate the interlayer region of organo-LDH, pushing apart the metal hydroxide sheets and form an intercalated structure. With time, more and more polymer chains enter the interlayer region and the shear force from melt blending induces the delamination of the surface layers one by one from the surface of organo-LDH particle [\[16\]](#). Exfoliated nanoscale sheets and intercalated structures can occur in nanocomposites at the same time.

The TEM images of bulk polymerized polymer/HDEHP-LDH composites with 5% organo-LDH loading are shown in [Fig. 9](#). With both PS and PMMA one only observes agglomerates, indicating that an immiscible system is formed by bulk polymerization. As noted above, the polarity of the LDH makes it very difficult to disperse in a solvent or the monomer and thus it is not surprising that immiscibility is observed.

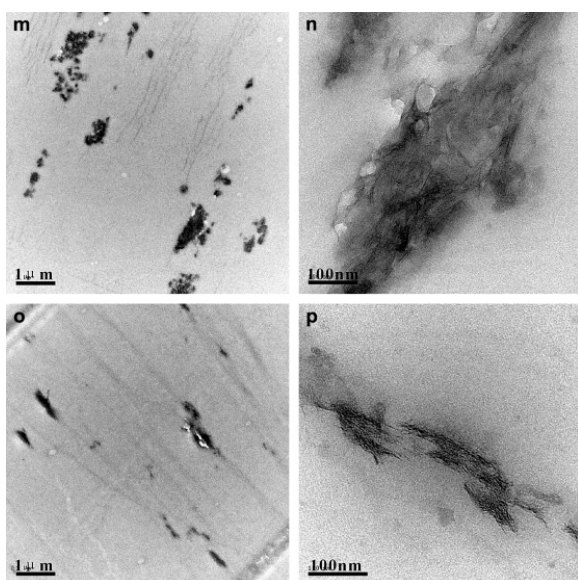


Fig. 9. TEM micrographs of bulk polymerization composites made with the phosphate LDH, HDEHP. (m, n) PMMA and (o, p) PS. The low magnification image is shown on the left with the higher magnification image on the right.

### 3.2.3. Mechanical properties

The tensile strength and elongation at break of melt blended PMMA and PS nanocomposites are shown in [Table 2](#). Both the tensile strength and the elongation at break are relatively constant for all compositions that have been studied here. This is very unlike the situation for MMT nanocomposites of either PMMA or PS where an exfoliated nanocomposite gives enhanced mechanical properties. In previous work from these laboratories, we have routinely observed that the mechanical properties were not enhanced with LDHs and have suggested that this maybe due to smaller length of the organo-LDH, which provides less reinforcement than is obtained when MMT is used [\[12\]](#), [\[13\]](#).

Table 2. Mechanical properties of PMMA and PS nanocomposites.

Formulation	Tensile strength (MPa)	Elongation at break (%)
PMMA	30 ± 6	3.2 ± 0.5
PMMA + 3% HDEHP-LDH	30 ± 6	3.5 ± 0.8
PMMA + 5% HDEHP-LDH	33 ± 5	4.0 ± 2.0
PMMA + 10% HDEHP-LDH	26 ± 7	3.6 ± 1.5
PMMA + 3% SDBS-LDH	34 ± 5	3.8 ± 1.0
PMMA + 5% SDBS-LDH	30 ± 4	3.4 ± 0.4
PMMA + 10% SDBS-LDH	28 ± 6	3.6 ± 1.0
PMMA + 3% SEHS-LDH	27 ± 4	2.7 ± 0.1
PMMA + 5% SEHS-LDH	39 ± 9	3.8 ± 1.6
PMMA + 10% SEHS-LDH	42 ± 5	3.9 ± 0.6
PS	32 ± 3	2.9 ± 0.2
PS + 3% HDEHP-LDH	32 ± 9	3.2 ± 0.4
PS + 5% HDEHP-LDH	31 ± 6	3.5 ± 1.3
PS + 10% HDEHP-LDH	30 ± 3	3.0 ± 0.2
PS + 3% SDBS-LDH	31 ± 10	2.9 ± 0.4
PS + 5% SDBS-LDH	30 ± 8	2.9 ± 0.5
PS + 10% SDBS-LDH	27 ± 6	2.9 ± 0.4
PS + 3% SEHS-LDH	30 ± 4	2.9 ± 0.1
PS + 5% SEHS-LDH	30 ± 3	3.2 ± 1.3

PS + 10% SEHS-LDH	24 ± 9	2.7 ± 0.4
-------------------	--------	-----------

### 3.2.4. Thermal stability of the nanocomposites

A very important characteristic of polymers is their thermal stability at elevated temperatures. Fig. 10 shows the thermogravimetric analysis traces of pure PMMA and PS and their nanocomposites with 10% organo-LDH loading. The degradation of PMMA follows a two-step process. The onset temperatures of the two steps are at 290 °C and 393 °C, respectively. The first step is due to the degradation of unsaturated chain ends and the second to random scission within the polymer chains [23], [24]. The first peak is more pronounced in virgin PMMA than in any of the composites and the temperature at which degradation occurs increases, *i.e.*, the presence of the LDH causes some thermal stabilization of the PMMA. Table 3 shows a summary of the TGA data, including the onset temperature of degradation, as measured by temperature at which 10% of the sample is lost,  $T_{0.1}$ ; the temperature at which 50% mass is lost, the mid-point temperature  $T_{0.5}$ ; and the fraction of the non-volatile residue remaining at 600 °C, labeled as char. The onset temperature of the degradation is slightly increased in the PMMA composites as is the temperature of 50% degradation; this is the expected behavior for a well-dispersed MMT in PMMA and indicates that when there is some amount of nano-dispersion, the thermal stability is enhanced [25], [26], [27]. The amount of residue is slightly larger than what might be expected based only on the LDH content; it is possible that some charring of the polymer occurs and the residue consists of both carbonaceous char from the polymer along with LDH residue.

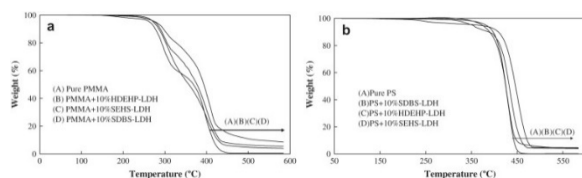


Fig. 10. TGA curves of PMMA composites (a) and PS composites (b).

Table 3. TGA summary results for PMMA and PS and their nanocomposites.

Formulation	$T_{0.1}$ (°C)	$T_{0.5}$ (°C)	Char (%)
Pure PMMA	276	368	0.6
PMMA + 10% HDEHP-LDH	286	358	4.0
PMMA + 10% SEHS-LDH	289	377	5.5
PMMA + 10% SDBS-LDH	298	393	8.6
Pure PS	394	424	0.1
PS + 10% SDBS-LDH	374	416	4.3
PS + 10% SEHS-LDH	366	425	4.9
PS + 10% HDEHP-LDH	375	430	4.1

The decomposition of PS system follows a single step; the onset temperature of the degradation decreases when the organo-LDH is present as does  $T_{0.5}$ . This is again unlike what is usually seen with MMT systems where the addition of MMT brings about an increase in both  $T_{0.1}$  and  $T_{0.5}$  [25], [26], [27]. Based on the fraction of non-volatile in each organo-LDH, one might expect to obtain between 3 and 5% residue in these composites and the experimental amount is in this range, so it appears that all residues are due only to the presence of the LDH.

### 3.2.5. Fire retardancy of the nanocomposites

Cone calorimeter is widely used to evaluate the fire performance of polymers. The parameters that may be evaluated from cone calorimetry include the heat release rate (HRR), and especially its peak value (PHRR); the time to ignition ( $t_{ig}$ ); the volume of smoke (VOS); the total heat released (THR), a measure of the extent to which the entire polymer burns; and the average mass loss rate (AMLR). The parameter that has been given the greatest attention in fire retardancy is the peak heat release rate, which gives information about the size of the

fire and can be viewed as the “driving force” of the fire. From MMT systems, it is known that the reduction in the PHRR is usually correlated with a decrease in the mass loss rate, *i.e.*, the change in the rate at which mass is lost dictates the heat release rate [25], [26], [27].

The cone calorimetric data for the PMMA composites, obtained at heat flux of 50 kW/m<sup>2</sup>, is shown in Table 4 and Fig. 11. For the melt blended systems, all three additives give a significant reduction in the PHRR at 10% LDH loading, but there is a large difference between the various additives. For the phosphate, which is well-dispersed, the reductions are quite similar at 3, 5 and 10%, respectively the reductions are 29, 33 and 37% and these all fall within the normal  $\pm 10\%$  error bars for cone calorimetry. On the other hand, for the sulfonate there is a large variation depending upon loading ranging from a 17% reduction at 3% loading to 45% at 10% loading. This system may also be said to be well-dispersed but it is obvious that there is a significant difference between these two. The sulfate, which is not well-dispersed, gives the lowest reduction in the PHRR and its performance at 10% loading is actually poorer than that of the phosphate at 3% loading. Nonetheless, at 10% loading this poorly dispersed system still gives a 27% reduction in the PHRR. This is much larger than is to be expected for a microcomposite and is indicative of another mechanism of fire retardancy from these materials other than the barrier mechanism which is usually ascribed to nanocomposite formation [28]. The likely pathways by which a poorly dispersed LDH can affect fire retardancy are the endothermic decomposition of the magnesium and aluminum hydroxides and the evolution of water which will dilute the volatile materials. One may attribute the reduction in the PHRR with the sulfate to this process and thus the additional reduction for the phosphate and sulfonate may be attributed to the dispersion of these materials.

Table 4. Cone calorimetric data for PMMA and its composites.

	Formulation	PHRR (kW/m <sup>2</sup> )	Reduction (%)	THR (MJ/m <sup>2</sup> )	VOS (L)	AMLR (g/s m <sup>2</sup> )	t <sub>ig</sub> (s)
Melt blending	Pure PMMA	1109 ± 47	NA	80 ± 1	460 ± 45	35 ± 3	13 ± 3
	PMMA + 3% SDBS-LDH	915 ± 26	17	77 ± 1	520 ± 20	44 ± 4	10 ± 1
	PMMA + 5% SDBS-LDH	790 ± 31	29	76 ± 0	623 ± 25	10 ± 0	12 ± 1
	PMMA + 10% SDBS-LDH	615 ± 5	45	72 ± 1	809 ± 55	7 ± 3	9 ± 2
	PMMA + 3% HDEHP-LDH	784 ± 51	29	76 ± 1	380 ± 50	27 ± 1	14 ± 1
	PMMA + 5% HDEHP-LDH	739 ± 53	33	75 ± 0	451 ± 30	26 ± 1	12 ± 2
	PMMA + 10% HDEHP-LDH	703 ± 15	37	73 ± 2	715 ± 3	17 ± 1	8 ± 0
	PMMA + 3% SEHS-LDH	974 ± 60	12	79 ± 0	340 ± 55	28 ± 5	11 ± 1
	PMMA + 5% SEHS-LDH	901 ± 7	19	78 ± 1	373 ± 20	24 ± 3	12 ± 1
Bulk polymerization	PMMA + 10% SEHS-LDH	811 ± 13	27	74 ± 0	412 ± 35	41 ± 1	9 ± 0
	Pure PMMA	883 ± 30	NA	80 ± 1	1471 ± 400	35 ± 3	13 ± 3
	PMMA + 3% HDEHP-LDH	806 ± 40	9	78 ± 1	991 ± 350	28 ± 3	10 ± 2
	PMMA + 5% HDEHP-LDH	755 ± 60	15	77 ± 1	685 ± 150	27 ± 1	11 ± 1
	PMMA + 10% HDEHP-LDH	611 ± 30	31	74 ± 0	1454 ± 300	21 ± 2	9 ± 1

PHRR, peak heat release rate; % reduction,  $100 \times \text{PHRR}_{\text{polymer}} - \text{PHRR}_{\text{composite}} / \text{PHRR}_{\text{polymer}}$ ; THR, total heat released; VOS, volume of smoke produced during the combustion; AMLR, average mass loss rate;  $t_{ig}$ , time to ignition.

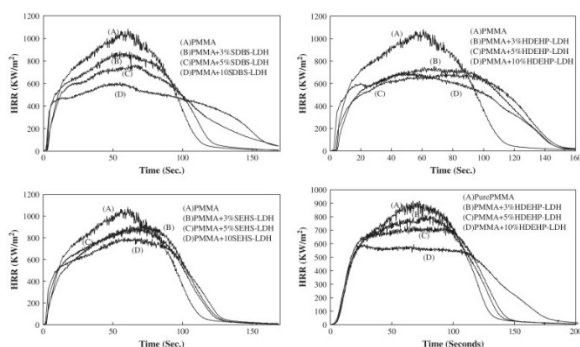


Fig. 11. HRR curves of melt blending composites: PMMA + SDBS-LDH, PMMA + HDEHP-LDH, PMMA + SEHS-LDH, and bulk polymerization PMMA + HDEHP-LDH.

For the bulk polymerized material, which is not well-dispersed, the reductions in the PHRR are similar to those of the sulfate by melt blending and thus one may attribute any effect to the endothermic decomposition and concomitant formation of water. These results, only the phosphate was used, are also shown in [Table 4](#) and [Fig. 11](#).

The results for polystyrene, obtained at a flux of  $35 \text{ kW/m}^2$ , are provided in [Table 5](#) and [Fig. 12](#). Here the best dispersion is obtained with the sulfonate and so these results will be discussed first. There is very little dependence on the amount of the LDH for the sulfonate, the reductions are 40, 44 and 49 at 3, 5 and 10%, respectively. This reduction is comparable to that seen with PS–MMT systems and is indicative of good dispersion and good fire retardancy [\[25\]](#), [\[26\]](#). Neither the sulfate nor the phosphate is well-dispersed and both show lower reductions in the PHRR but the phosphate reduction, about 30% and invariant to amount of LDH, is much larger than that for the sulfate. One may once again attribute the reduction in the sulfate to the microcomposite effect of the LDH and thus there is some effect due to nano-dispersion in the sulfonate and, surprisingly, also in the phosphate. As with PMMA, bulk polymerization does not give good dispersion and the reductions in the PHRR are roughly comparable to those with the sulfate, thus fire retardancy in this microcomposite is due to the endothermic decomposition and water release.

Table 5. Cone calorimetric data for PS and its composites.

Melt blending	Pure PS	$1599 \pm 76$	NA	$115 \pm 2$	$3765 \pm 130$	$37 \pm 4$	$46 \pm 2$
	PS + 3% SDBS-LDH	$954 \pm 25$	40	$106 \pm 1$	$3830 \pm 30$	$23 \pm 4$	$26 \pm 2$
	PS + 5% SDBS-LDH	$893 \pm 35$	44	$105 \pm 0$	$4021 \pm 60$	$18 \pm 0$	$27 \pm 1$
	PS + 10% SDBS-LDH	$817 \pm 99$	49	$89 \pm 17$	$3900 \pm 30$	$19 \pm 2$	$20 \pm 11$
	PS + 3% HDEHP-LDH	$1125 \pm 20$	30	$96 \pm 1$	$3602 \pm 40$	$25 \pm 7$	$32 \pm 1$
	PS + 5% HDEHP-LDH	$1094 \pm 23$	32	$98 \pm 2$	$3661 \pm 100$	$27 \pm 4$	$25 \pm 4$
	PS + 10% HDEHP-LDH	$1076 \pm 9$	33	$85 \pm 18$	$3695 \pm 50$	$28 \pm 1$	$22 \pm 1$
	PS + 3% SEHS-LDH	$1381 \pm 49$	14	$114 \pm 2$	$3727 \pm 75$	$29 \pm 1$	$28 \pm 2$
	PS + 5% SEHS-LDH	$1402 \pm 38$	12	$114 \pm 0$	$3854 \pm 30$	$30 \pm 2$	$21 \pm 1$
	PS + 10% SEHS-LDH	$1088 \pm 160$	32	$110 \pm 3$	$4062 \pm 40$	$25 \pm 1$	$19 \pm 2$
Bulk polymerization	Pure PS	$1260 \pm 38$	NA	$99 \pm 3$	$3844 \pm 420$	$26 \pm 7$	$50 \pm 1$
	PS + 3% HDEHP-LDH	$1201 \pm 18$	5	$103 \pm 2$	$3380 \pm 500$	$26 \pm 3$	$22 \pm 3$
	PS + 5% HDEHP-LDH	$1181 \pm 13$	6	$105 \pm 3$	$3238 \pm 270$	$29 \pm 2$	$13 \pm 1$
	PS + 10% HDEHP-LDH	$1002 \pm 30$	17	$101 \pm 1$	$2986 \pm 250$	$22 \pm 1$	$14 \pm 1$

PHRR, peak heat release rate; % reduction,  $100 \times \text{PHRR}_{\text{polymer}} - \text{PHRR}_{\text{composite}} / \text{PHRR}_{\text{polymer}}$ ; THR, total heat released; VOS, volume of smoke produced during the combustion; AMLR, average mass loss rate;  $t_{ig}$ , time to ignition.

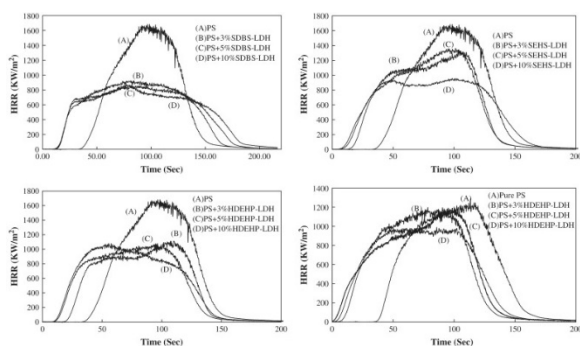


Fig. 12. Heat release rate curves for PS + SDBS-LDH, PS + SEHS-LDH, PS + HDEHP-LDH and the bulk polymerized PS-HDEHP-LDH.

For both polymers, the decrease in the mass loss rate is much larger than the decrease in the PHRR, which is contrary to what is typically seen in MMT systems. This suggests that while there may be a strictly nanocomposite effect, something else is happening in these systems which has unusual effects (compared to MMT). Further work is in progress to understand this [25], [26], [27].

The total heat released (THR) is constant for PMMA and the (nano)composites, as is normally observed for MMT systems, which indicates that essentially all of the polymer burns [26]. As is also typical for PMMA nanocomposites, the time to ignition is not appreciably shortened by the presence of the organo-LDH, unlike the observation with other polymers.

For the melt blended PMMA systems, the volume of smoke is approximately constant, except at 10% LDH loading where it is marginally increased. Surprisingly, the bulk polymerized PMMA samples produce much more smoke and exhibit much larger error bars than expected. This may indicate the presence of some residual monomer in the samples.

The mass of the residue corresponds rather well to the initial content of the organo-LDH; as the LDH loading increases the mass of residue increases. The char structure is a little different with each polymer and with each of the organo-LDHs. For both PMMA and PS, more of the aluminum foil in which the cone sample is wrapped is covered at the end of the run and the structure is more cohesive; with PMMA this char covers essentially the entire pan and is puffy, white in appearance. With PS, there are some black specks interspersed and somewhat less of the pan is covered. For the phosphate with PMMA, the char is a crusty black material which covers around 60% of the sample pan while, with PS the appearance is similar but much less of the pan, perhaps 20%, is covered. For the sulfate, which had the poorest dispersion with both polymers, there are only a few small pieces of black char with both polymers. When the phosphate was used and the composites made by bulk polymerization, the residue is similar in appearance to that by melt blending but there is less material. Photographs of the residues are provided in Fig. 13. Nanocomposites, in general, retain their shape after burning and this suggests that the sulfonate, which seems to best retain its shape, may have been the most well-dispersed LDH in either polymer [29]. While this is not in complete agreement with the TEM images, the sulfonate does show nano-dispersion by TEM.

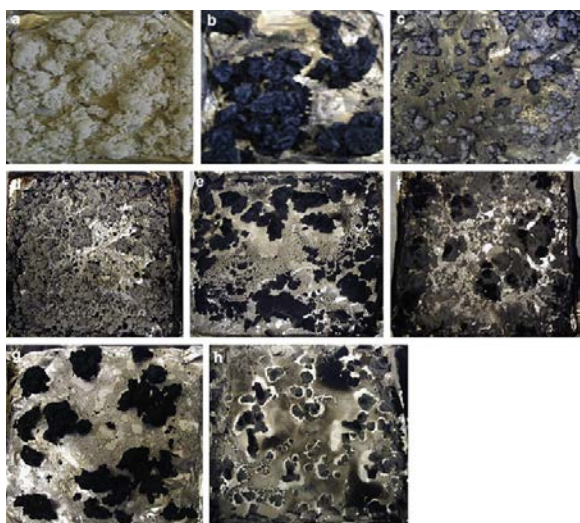


Fig. 13. The residue photographs of: PMMA and PS nanocomposites with 10% organo-LDH loading: (a) melt blending PMMA + SDBS-LDH, (b) melt blending PMMA + HDEHP-LDH, (c) melt blending PMMA + SEHS-LDH, (d) melt blending PS + SDBS-LDH. (e) Melt blending PS + HDEHP-LDH, (f) melt blending SEHS-LDH; (g) bulk polymerization PMMA + 10% HDEHP-LDH, (h) bulk polymerization PS + 10% HDEHP-LDH.

## 4. Conclusions

The basal spacing of SDBS-LDH, SEHS-LDH and HDEHP-LDH increased from 0.77 nm for the pristine inorganic LDH to 2.90 nm, 2.14 nm and 2.34 nm, respectively, and these organically-modified LDHs exhibit a highly ordered interlayer anion arrangement. It is much easier to disperse these materials in PMMA than in PS but the sulfate, SEHS, does not disperse well in either polymer. The mechanical properties are not enhanced at all by the addition of these organo-LDHs but they do show enhanced fire properties. With both PMMA and PS, a reduction in the peak heat release rate of about 50% is seen using the sulfonate-LDH. In the case of PMMA, this is a well-dispersed system at the nanometer level but in PS the dispersion as accessed by TEM is not as good.

## Acknowledgments

Partial support for this work by the US Department of Commerce, National Institute of Standards and Technologies, Grant 60NANB6D6018 is gratefully acknowledged.

## References

- [1] F. Leroux, J.P. Besse **Polymer interleaved layered double hydroxide: a new emerging class of nanocomposites** *Chem Mater*, 13 (2001), pp. 3507-3515
- [2] W. Chen, L. Feng, B.J. Qu **Preparation of nanocomposites by exfoliation of ZnAl layered double hydroxides in nonpolar LLDPE solution** *Chem Mater*, 16 (2004), pp. 368-370
- [3] H.T. Zhao, L.N. Kathryn **Dodecyl sulfate-hydrotalcite nanocomposites for trapping chlorinated organic pollutants in water** *J Colloid Interface Sci*, 274 (2004), pp. 613-624
- [4] F. Cavani, F. Trifiro, A. Vaccari **Hydrotalcite-type anionic clays: preparation, properties and applications** *Catalysis Today*, 11 (1991), pp. 173-301
- [5] C. Forano, T. Hibino, F. Leroux, C. Taviot-Gueho **Layered double hydroxides** F. Bergaya, B.K.G. Theng, G. Lagaly (Eds.), *Handbook of clay science*, Elsevier (2006), pp. 1021-1095
- [6] K.L. Erickson, T.E. Bostrom, R.L. Frost **A study of structural memory effects in synthetic hydrotalcites using environmental SEM** *Mater Lett*, 59 (2005), pp. 226-229
- [7] M. Zammarano, M. Franceschi, S. Bellayer, J.W. Gilman, S. Meriani **Preparation and flame resistance properties of revolutionary self-extinguishing epoxy nanocomposites based on layered double hydroxides** *Polymer*, 46 (2005), pp. 9314-9328



- [8] M.C. Costache, M.J. Heidecker, E. Manias, G. Camino, A. Frache, G. Beyer, *et al.* **The influence of carbon nanotubes, organically modified montmorillonites and layered double hydroxides on the thermal degradation and fire retardancy of polyethylene, ethylene–vinyl acetate copolymer and polystyrene** *Polymer*, 48 (2007), pp. 6532-6545
- [9] G.A. Wang, C.C. Wang, C.Y. Chen **The disorderly exfoliated LDHs/PMMA nanocomposite synthesized by in situ bulk polymerization** *Polymer*, 46 (2005), pp. 5065-5074
- [10] Z.P. Xu, P.S. Braterman **Competitive intercalation of sulfonates into layered double hydroxides (LDHs): the key role of hydrophobic interactions** *J Phys Chem C*, 111 (2007), pp. 4021-4026
- [11] N. Desrosiers, J. Pison, Y. Israeli, C. Taviot-Gueho, J.-P. Besse, J.-P. Morel **Intercalation of dicarboxylate anions into a Zn–Al–Cl layered double hydroxide: microcalorimetric determination of the enthalpies of anion exchange** *J Mater Chem*, 13 (2003), pp. 2582-2590
- [12] C. Manzi-Nshuti, D. Wang, J.M. Hossenlopp, C.A. Wilkie **Aluminum-containing layered double hydroxides: the thermal, mechanical and fire properties of (nano)composites of poly(methyl methacrylate)** *J Mater Chem*, 18 (2008), pp. 3091-3102
- [13] C. Nyambo, P. Songtipya, E. Manias, M. Jimenez-Gasco, C.A. Wilkie **Effect of MgAl-layered double hydroxide exchanged with linear alkyl carboxylates on fire retardancy of PMMA and PS** *J Mater Chem*, 18 (2008), pp. 4827-4838
- [14] Manzi-Nshuti C, Wang D, Hossenlopp JM, Wilkie CA. The role of the trivalent metal in an LDH: synthesis, characterization and fire properties of the thermally stable PMMA/LDH system, *Polym Degrad Stab*, in press. doi:10.1016/polymdegradstab.2008.12.012.
- [15] B. Wang, H. Zhang, D.G. Evans, X. Duan **Surface modification of layered double hydroxides and incorporation of hydrophobic organic compounds** *Mater Chem Phys*, 92 (2005), pp. 190-196
- [16] F.R. Costa, M. Saphiannikova, U. Wagenknecht **Layered double hydroxide based polymer nanocomposites** *Adv Polym Sci*, 210 (2008), pp. 101-168
- [17] V.R.L. Constantino, T.J. Pinnavaia **Basic properties of  $Mg^{2+}_{1-x}Al^{3+}_x$  layered double hydroxides intercalated by carbonate, hydroxide, chloride, and sulfate anions** *Chem Mater*, 34 (1995), pp. 883-892
- [18] R.L. Frost, K.L. Erickson, T.J. Kloprogge **Vibrational spectroscopic study of the nitrate containing hydroxide intercalated layered double hydroxide** *Spectrochim Acta Part A*, 61 (2005), pp. 2919-2925
- [19] Z.P. Xu, P.S. Braterman **High affinity of dodecylbenzene sulfonate for layered double hydroxide and resulting morphological changes** *J Mater Chem*, 13 (2003), pp. 268-273
- [20] E. Kandare, J.M. Hossenlopp **Thermal degradation of acetate-intercalated hydroxy double and layered hydroxy salts** *Inorg Chem*, 45 (2006), pp. 3766-3773
- [21] J.Q. Wang, Z.D. Han **The combustion behavior of polyacrylate ester/graphite oxide composites** *Polym Adv Technol*, 17 (2006), pp. 335-340
- [22] D.Y. Wang, J. Zhu, Q. Yao, C.A. Wilkie **A comparison of various methods for the preparation of polystyrene and poly(methyl methacrylate) clay nanocomposites** *Chem Mater*, 14 (2002), pp. 3837-3843
- [23] S. Bandyopahyay, E.P. Giannelis, A.J. Hsieh **Thermal and thermo-mechanical properties of PMMA nanocomposites** *Polym Mater Sci Eng*, 82 (2000), pp. 476-478
- [24] T. Kashiwagi, A. Inaba, J.E. Brown, K. Hatada, T. Kitayama, E. Masuda **Effects of weak linkages on the thermal and oxidative degradation of poly(methyl methacrylates)** *Macromolecules*, 19 (1986), pp. 2160-2168
- [25] J. Zhu, C.A. Wilkie **Thermal and fire studies on polystyrene–clay nanocomposites** *Polym Int*, 49 (2000), pp. 1158-1163
- [26] J. Zhu, A.B. Morgan, F.J. Lamelas, C.A. Wilkie **Fire properties of polystyrene–clay nanocomposites** *Chem Mater*, 13 (2001), pp. 3774-3780
- [27] P. Jash, C.A. Wilkie **Effects of surfactants on the thermal and fire properties of poly(methyl methacrylate)/clay nanocomposites** *Polym Degrad Stab*, 88 (2005), pp. 401-406
- [28] J.W. Gilman, C.L. Jackson, A.B. Morgan, R. Harris Jr., E. Manias, E.P. Giannelis, *et al.* *Chem Mater*, 12 (2000), pp. 1866-1873

[\[29\]](#) B.N. Jang, C.A. Wilkie **The effects of clay on the thermal degradation behavior of poly(styrene-co-acrylonitrile)** *Polymer*, 46 (2005), pp. 9702-9713